

## Molecular Synchronization Waves in Arrays of Allosterically Regulated Enzymes

Vanessa Casagrande,<sup>1</sup> Yuichi Togashi,<sup>2,\*</sup> and Alexander S. Mikhailov<sup>2,†</sup>

<sup>1</sup>Hahn-Meitner-Institut, Glienicker Straße 100, 14109 Berlin, Germany

<sup>2</sup>Fritz-Haber-Institut der Max-Planck-Gesellschaft, Faradayweg 4-6, 14195 Berlin, Germany

(Received 12 March 2007; published 23 July 2007)

Spatiotemporal pattern formation in a product-activated enzymic reaction at high enzyme concentrations is investigated. Stochastic simulations show that catalytic turnover cycles of individual enzymes can become coherent and that complex wave patterns of molecular synchronization can develop. The analysis based on the mean-field approximation indicates that the observed patterns result from the presence of Hopf and wave bifurcations in the considered system.

DOI: [10.1103/PhysRevLett.99.048301](https://doi.org/10.1103/PhysRevLett.99.048301)

PACS numbers: 82.40.Ck, 05.45.Xt, 82.39.Fk, 87.18.Pj

Molecular machines, such as molecular motors, ion pumps, and some enzymes, play a fundamental role in biological cells and also can be used in the emerging soft-matter nanotechnology [1]. A protein machine is a cyclic device, where each cycle consists of conformational motions initiated by binding of an energy-bringing ligand [2,3]. In motors, such internal motions generate mechanical work [4], while in enzymes they enable or facilitate chemical reaction events (see, e.g., [5,6]). Much attention has been attracted to studies of biomembranes with ion pumps and molecular motors, where membrane instabilities and synchronization effects have been analyzed [7–9]. Here, a different class of distributed active molecular systems—formed by enzymes—is considered. The catalytic activity of an allosteric enzyme protein is activated or inhibited by binding of small regulatory molecules; the role of such regulatory molecules can be played by products of the same reaction [10]. Previous investigations of simple product-regulated enzymic systems [11,12] and enzymic networks [13] in small spatial volume with full diffusional mixing have shown that spontaneous synchronization of molecular turnover cycles can take place there. External molecular synchronization of enzymes of the photosensitive P-450 dependent monooxygenase system by periodic optical forcing has been experimentally demonstrated [14].

In this Letter, spatiotemporal pattern formation in enzymic arrays is investigated. In such systems, immobile enzymes are attached to a solid planar support immersed into a solution through which fresh substrate is supplied and product molecules are continuously removed. Product molecules released by an enzyme diffuse through the solution and activate catalytic turnover cycles of neighboring enzymes in the array.

A simple stochastic model [12] of an enzyme as a cyclic machine (a stochastic phase oscillator), shown in Fig. 1, is used. Binding of a substrate molecule to an enzyme  $i$  initiates an ordered internal conformational motion, described by the conformational phase coordinate  $\phi_i$ . The initial state corresponds to the phase  $\phi_i = 0$ . The catalytic

conversion event takes place and the product is released at the state  $\phi_p$  inside the cycle. After that, the conformational motion continues until the equilibrium state of the enzyme ( $\phi_i = 1$ ) is finally reached. Initiation of a turnover cycle is a random event, occurring at a certain probability rate. We assume that substrate is present in abundance, and its concentration is not affected by the reactions. Conformational motion inside the cycle is modeled as a stochastic diffusional drift process, described by equation  $\dot{\phi}_i = v + \eta_i(t)$ , where  $v$  is the mean drift velocity and  $\eta_i(t)$  is an internal white noise with  $\langle \eta_i(t)\eta_j(t') \rangle = 2\sigma\delta_{ij}\delta(t-t')$  where  $\sigma$  specifies intensity of intramolecular fluctuations.

Allosterically activated enzymes possess a site on their surface where regulatory molecules can become bound. Binding of a regulatory molecule leads to conformational change that enhances catalytic activity of the enzyme. A regulatory molecule binds to an enzyme with rate constant  $\beta$  and dissociate from it with rate constant  $\kappa$ . Binding of a regulatory molecule at an enzyme raises its probability to start a cycle from  $\alpha_0$  to  $\alpha_1$ . We assume that a regulatory molecule can bind to an enzyme only in its rest state and this molecule is released when the cycle is started. The role of regulatory molecules is played by product molecules of the same reaction. Immobile enzymes are randomly distributed in space with concentration  $c$ . Product diffuses at diffusion constant  $D$  and undergoes decay at rate constant

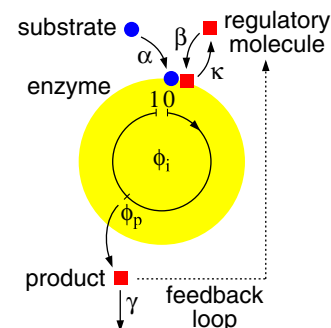


FIG. 1 (color online). A sketch of the model.

$\gamma$ . The characteristic diffusion length of product molecules is  $l_{\text{diff}} = \sqrt{D/\gamma}$ .

In our stochastic 2D simulations, the medium was discretized into spatial cells (up to  $256 \times 256$ ), each containing a number of enzyme molecules. The cells were so small that diffusional mixing of product molecules in a cell within the shortest characteristic time of the reaction could always take place. Each enzyme was described by the stochastic model given above; diffusion of product molecules was modeled as a random walk over a discrete cell lattice. The mean cycle time  $\tau = 1/\nu$  was chosen as the time unit ( $\tau = 1$ ). Systems including up to 655 360 enzymes were used in the simulations.

Figures 2(a) and 2(b) (see also videos 1 and 2 in Ref. [15]) show two typical examples of stochastic 2D simulations. Here, spatial distributions of product molecules are displayed. Waves of product concentration are propagating through the medium. In a peak of a wave, many locally present enzymes are simultaneously releasing product molecules. Since product release can take place only at a certain stage inside the cycle, this means that the cycles of enzymes are locally synchronized. Not only regular wave structures, such as rotating spiral waves or target patterns [Fig. 2(a)], but also complex regimes of wave turbulence [Fig. 2(b)] have been observed.

To understand and interpret stochastic simulation results, an analytical study of the system in the mean-field approximation, which holds in the limit of high enzyme concentrations, has been performed. In this approximation, the system is characterized by three continuous variables  $n_0(\mathbf{r}, t)$ ,  $n_1(\mathbf{r}, t)$ , and  $m(\mathbf{r}, t)$ , which represent local concentrations of enzymes in the rest state without or with regulatory molecules attached ( $n_0$  and  $n_1$ ) and local concentration of the product ( $m$ ). For simplicity, internal fluctuations in enzymes are neglected ( $\sigma = 0$ ). Thus, all enzymes which have started their cycles at some time  $t$  would release their products at a definite time  $t + \tau_p$  (with  $\tau_p = \phi_p/\nu$ ) and finish their cycles, returning to the rest state, at time  $t + \tau$ . Therefore, the system is described by a set of three reaction-diffusion equations with time delays:

$$\frac{\partial n_1}{\partial t} = \beta m n_0 - \kappa n_1 - \alpha_1 n_1, \quad (1a)$$

$$\frac{\partial n_0}{\partial t} = -\beta m n_0 + \kappa n_1 - \alpha_0 n_0 + \alpha_0 n_0(t - \tau) + \alpha_1 n_1(t - \tau), \quad (1b)$$

$$\frac{\partial m}{\partial t} = -\beta m n_0 + \kappa n_1 + \alpha_1 n_1 - \gamma m + \alpha_0 n_0(t - \tau_p) + \alpha_1 n_1(t - \tau_p) + D \nabla^2 m. \quad (1c)$$

The system always has a uniform stationary state with certain concentrations  $\bar{n}_0$ ,  $\bar{n}_1$ , and  $\bar{m}$ , which can be found as solutions of the respective algebraic equations. This state corresponds to the absence of synchronization. However, it may become unstable if allosteric activation is strong

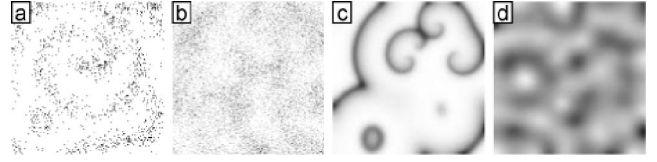


FIG. 2. Stochastic (a),(b) and mean-field (c),(d) simulations of 2D wave patterns: (a)  $\tau_p = 0.14$ ,  $c = 1$ , and  $\beta = 300$ ; (b)  $\tau_p = 0.25$ ,  $c = 10$ , and  $\beta = 10$ ; (c)  $\tau_p = 0.14$ ,  $c = 1$ , and  $\beta = 300$ ; (d)  $\tau_p = 0.34$ ,  $c = 100$ , and  $\beta = 1.42$ . Other parameters are  $\alpha_0 = 1$ ,  $\alpha_1 = 1000$ ,  $\kappa = 10$ ,  $\gamma = 10$ ,  $\sigma = 0$ ,  $D = 100$ . The linear size of the shown area is  $L = 40 l_{\text{diff}}$  in all panels.

enough. To analyze stability, small perturbations  $\delta n_0$ ,  $\delta n_1$ , and  $\delta m$  are added to the stationary state, Eqs. (1) are linearized and their solutions are sought as  $\delta n_0 \sim \delta n_1 \sim \delta m \sim \exp(\lambda_q t - i q x)$  with  $\lambda_q = \mu_q + i \omega_q$ . Thus, each spatial mode with wave vector  $q$  is characterized by its frequency  $\omega_q$  and its rate of growth  $\mu_q$ . The properties  $\mu_q$  and  $\omega_q$  are given by the roots of a characteristic equation which is determined by the linearization matrix of Eqs. (1). The steady state becomes unstable when at least one spatial mode with some wave number  $q_0$  starts to grow ( $\mu_{q_0} > 0$ ).

As the bifurcation parameter, coefficient  $\beta$  can be chosen. If regulatory molecules cannot bind to enzymes ( $\beta = 0$ ), feedback is absent and instabilities are not possible. On the other hand, allosteric activation becomes strong if regulatory molecules can easily bind and, in this case, emergence of oscillations and wave patterns can be expected. Our bifurcation analysis reveals that, depending on the parameters of the system, it can exhibit either a Hopf or a wave bifurcation [16]. As a result of the Hopf bifurcation, uniform oscillations with  $q = 0$  develop. Because of the presence of delays in Eqs. (1), the characteristic equation is nonpolynomial in terms of  $\lambda$  and, generally, a number of oscillatory solutions with different frequencies  $\omega$  are possible. Physically, such solutions correspond to formation of several synchronous enzymic groups. This effect has been previously extensively investigated for similar systems in small spatial volumes with full diffusional mixing [11], and we shall not further discuss it here. The most robust uniform oscillations, which we consider, are characterized by the frequency  $\omega \approx 2\pi/\tau$  and correspond to the single-group synchronization. As the result of a wave bifurcation (also known as the Hopf bifurcation with a finite wave number [17]), the first unstable modes are traveling waves with a certain wave number  $q_0$ . Figure 3 shows the bifurcation diagram in the parameter plane ( $\tau_p, \beta$ ). Note the presence of a codimension-2 bifurcation point where the boundaries of the Hopf and the wave bifurcations join.

To investigate nonlinear dynamics of the system, numerical simulations of Eqs. (1) have been performed [16]. The explicit Euler integration method has been used; no-flux boundary conditions were applied. Results of 1D simulations are summarized in Fig. 3, and examples of

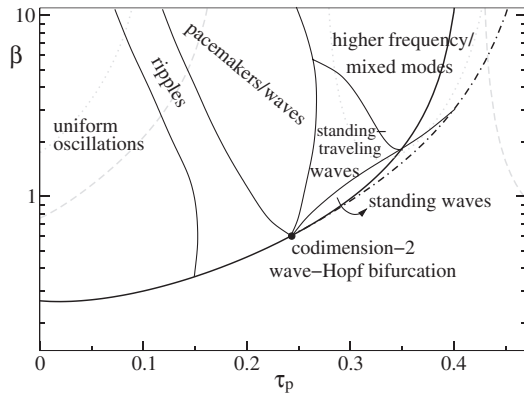


FIG. 3. Phase diagram ( $\alpha_0 = 1$ ,  $\alpha_1 = 1000$ ,  $\kappa = 10$ ,  $\gamma = 10$ ,  $c = 100$ ,  $D = 1000$ ). The Hopf bifurcation (solid line) and the wave bifurcation (dash-dotted line) boundaries are displayed. Gray lines show instability of the stationary state with respect to development of uniform oscillations with two (dashed) and three (dotted) groups in the well-mixed case. Lines separating parameter domains with different kinds of patterns are hand drawn, based on numerical simulations.

typical observed patterns are shown in Fig. 4. Standing waves [Fig. 4(a)] develop when the boundary of the wave bifurcation (dash-dotted curve) is crossed and uniform oscillations are observed above the boundary of the Hopf bifurcation. Near the codimension-2 point, more complex behavior was found. This included rippled oscillations [Fig. 4(b)], self-organized pacemakers [Fig. 4(c)], and modulated traveling waves [Fig. 4(d)]. The observed patterns are similar to those previously found in reaction-diffusion systems with the wave bifurcation [18]. In the right upper corner of the diagram in Fig. 3, higher fre-

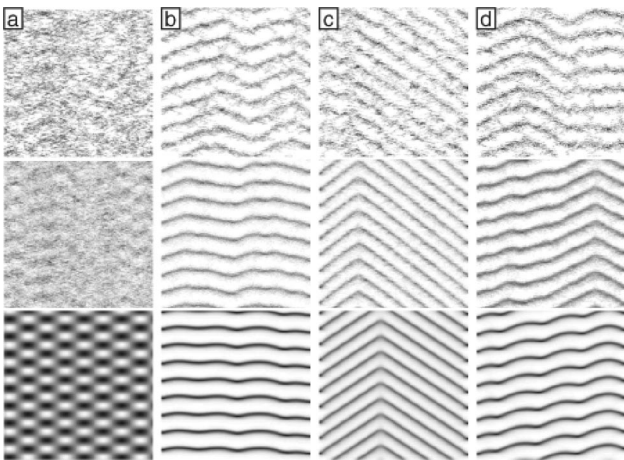


FIG. 4. Spatiotemporal patterns in a 1D system (in each panel, the vertical axis is time, running down, and the horizontal axis is the coordinate). The upper two rows are stochastic simulations ( $\sigma = 0$ ) with concentrations  $c = 1$  and  $c = 10$ , the bottom row shows mean-field simulations with  $c = 100$ . (a)  $\tau_p = 0.3$ ,  $\beta = 95/c$ ; (b)  $\tau_p = 0.14$ ,  $\beta = 260/c$ ; (c)  $\tau_p = 0.22$ ,  $\beta = 600/c$ ; (d)  $\tau_p = 0.16$ ,  $\beta = 300/c$ . Other parameters as in Fig. 3; the system size shown is  $L = 51 l_{\text{diff}}$ .

quency oscillations with several synchronous groups take place.

Two-dimensional simulations of reaction-diffusion equations (1) with time delay have been performed for selected parameter values. In 2D simulations, spontaneously developing concentric waves (target patterns) and spiral waves have been observed; target patterns were, however, unstable and evolved into pairs of rotating spiral waves [Fig. 2(c) and video 3 [15]]. Complex wave regimes, which can be qualitatively characterized as turbulence of standing waves, have also been observed [Fig. 2(d) and video 4 [15]].

The mean-field approximation is based on neglecting statistical fluctuations in concentrations of reacting species [11] and, therefore, it should hold in the high concentration limit. In Fig. 4, two upper panel rows display spatiotemporal patterns which are observed in stochastic simulations with parameter values corresponding to the respective mean-field simulations. To compare mean-field simulations with different enzyme densities, the following property of Eqs. (1) can be used: introducing relative concentrations  $\tilde{n}_0 = n_0/c$ ,  $\tilde{n}_1 = n_1/c$ , and  $\tilde{m} = m/c$ , it can be noticed that they obey the same equations, but with a rescaled coefficient  $\tilde{\beta} = \beta c$ . Thus, essentially the same patterns are observed as long as the parameter combination  $\beta c$  remains constant. In the stochastic simulations in Fig. 4, the coefficient  $\beta$  has been increased to compensate for a decrease in the enzyme concentration. For larger enzyme concentrations, good agreement between mean-field predictions and stochastic simulations has been found. In the mean-field equations (1), intramolecular fluctuations are not taken into account ( $\sigma = 0$  and therefore each turnover cycle has the same fixed duration  $\tau$ ). Stochastic simulations have been, however, also performed when such fluctuations were present. Synchronization waves could still be found even at internal noise levels which corresponded to the mean relative dispersion  $\xi$  of turnover times of about 10% [with  $\xi = \langle \delta\tau^2 \rangle^{1/2} / \tau \simeq (2\sigma\tau)^{1/2}$ ].

Although the emphasis in this Letter is on the phenomena in two-dimensional enzymic arrays, analogous effects should be expected for three-dimensional systems representing aqueous enzymic solutions. The linear stability analysis, yielding Hopf and wave bifurcation boundaries (see Fig. 3), is valid also for the 3D geometry. We have performed preliminary stochastic simulations for thin solution layers with high enzyme concentrations and could observe synchronization patterns similar to those found for the enzymic arrays.

A product molecule, released by an enzyme, diffuses in the solution until it either binds, as a regulatory molecule, to another enzyme or undergoes a decay. Here, it should be taken into account that a regulatory molecule can bind to an allosteric enzyme only at a certain binding site of characteristic radius  $R$ . Using the theory of diffusion-controlled reactions, the average time  $t_{\text{transit}}$  after which a regulatory product would find a binding site of one of the

enzymes can be roughly estimated [11] as  $t_{\text{transit}} = 1/cDR$ , if enzymes are uniformly distributed inside the reaction volume with concentration  $c$ . Therefore, binding typically occurs within the distance  $L_{\text{corr}} = (Dt_{\text{transit}})^{1/2} = (cR)^{-1/2}$  from the point where a molecule is released. Obviously, it can only take place if the product molecule has not undergone decay until that moment, i.e., if  $\gamma t_{\text{transit}} < 1$ . This condition puts a restriction on the enzyme concentration  $c$ , which must be higher than the critical concentration  $c^* = \gamma/DR$ . Choosing  $\gamma = 10^3 \text{ s}^{-1}$ ,  $D = 10^{-5} \text{ cm}^2 \text{ s}^{-1}$ , and  $R = 10^{-7} \text{ cm}$ , the critical enzyme concentration is  $c^* = 10^{15} \text{ cm}^{-3} = 10^{-6} \text{ M}$ . A similar estimate can be obtained when enzymes are immobilized on a plane immersed into a reactive solution; in this case the mean distance between the enzymes on the plane should be less than  $l_c = (Rl_{\text{diff}})^{1/2}$  [19]. Although the required enzyme concentrations are relatively large, they are within the range characteristic for biological cells (glycolytic enzymes are present [20] in a cell at even higher concentration of more than  $10^{-5} \text{ M}$ ). The characteristic temporal period of developing patterns is determined by the enzyme turnover time  $\tau$ , which typically varies from milliseconds to seconds. The characteristic length scale of developing wave patterns is determined by the diffusion length  $l_{\text{diff}}$ , which can vary under these conditions from a fraction of a micrometer to tens of micrometers.

Our analysis shows that spontaneous molecular synchronization of allosteric product-activated enzymes can be observed in enzymic arrays. Artificial arrays formed by immobilized protein machines (molecular motors) are already used in experiments on active nanoscale transport (see [21]). Many enzymes in biological cells are membrane bound, thus forming natural enzymic arrays. Similar phenomena are possible in dense enzyme solutions. In the study by Petty *et al.* [22], traveling waves of NAD(P)H and proton concentrations with the wavelength of about a micrometer were observed inside neutrophil cells. These metabolic waves had the temporal period of about 300 ms, which is by 2 orders of magnitude shorter than the characteristic period of glycolytic oscillations in the cells and lies closer to the time scales of turnover cycles of individual enzymes. An intriguing question, requiring further detailed analysis, is whether molecular synchronization waves may have already been seen in these experiments.

Molecular synchronization waves are principally different from classical concentration waves in reaction-diffusion systems. Under synchronization conditions, internal conformational states of individual enzyme molecules in their turnover cycles become strongly correlated. In optics, a similar situation is found when a transition to coherent laser generation has taken place. Our theoretical analysis may open a way to the investigations of a new class of spatiotemporal pattern formation in chemically active molecular systems.

The authors are grateful to M. Falcke and P. Stange for valuable discussions. Financial support of the Japan Society for the Promotion of Science for research abroad (Y. T.) is acknowledged.

\*Present address: Nanobiology Laboratories, Graduate School of Frontier Biosciences, Osaka University, 1-3 Yamadaoka, Suita, Osaka 565-0871, Japan.

togashi@phys1.med.osaka-u.ac.jp

†mikhailov@fhi-berlin.mpg.de

- [1] K. Kinbara and T. Aida, *Chem. Rev.* **105**, 1377 (2005).
- [2] L. A. Blumenfeld and A. N. Tikhonov, *Biophysical Thermodynamics of Intracellular Processes: Molecular Machines of the Living Cell* (Springer, Berlin, 1994).
- [3] M. Gerstein, A. M. Lesk, and C. Chothia, *Biochemistry* **33**, 6739 (1994).
- [4] F. Jülicher, A. Ajdari, and J. Prost, *Rev. Mod. Phys.* **69**, 1269 (1997).
- [5] H.-Ph. Lerch, A. S. Mikhailov, and B. Hess, *Proc. Natl. Acad. Sci. U.S.A.* **99**, 15410 (2002).
- [6] H.-Ph. Lerch, R. Rigler, and A. S. Mikhailov, *Proc. Natl. Acad. Sci. U.S.A.* **102**, 10807 (2005).
- [7] S. Ramaswamy, J. Toner, and J. Prost, *Phys. Rev. Lett.* **84**, 3494 (2000).
- [8] P. Lenz, J.-F. Joanny, F. Jülicher, and J. Prost, *Phys. Rev. Lett.* **91**, 108104 (2003).
- [9] H.-Y. Chen, *Phys. Rev. Lett.* **92**, 168101 (2004).
- [10] A. Goldbeter, *Biochemical Oscillations and Cellular Rhythms* (Cambridge University Press, Cambridge, 1996).
- [11] P. Stange, A. S. Mikhailov, and B. Hess, *J. Phys. Chem. B* **102**, 6273 (1998).
- [12] P. Stange, A. S. Mikhailov, and B. Hess, *J. Phys. Chem. B* **103**, 6111 (1999).
- [13] K. Sun and Q. Ouyang, *Phys. Rev. E* **64**, 026111 (2001).
- [14] M. Schienbein and H. Gruler, *Phys. Rev. E* **56**, 7116 (1997).
- [15] See EPAPS Document No. E-PRLTAO-99-041730 for dynamical evolutions of 2D wave patterns. Videos 1 to 4 correspond to panels (a) to (d) in Fig. 2, respectively. The linear size of the shown area is  $L = 81 L_{\text{diff}}$  (256 simulation cells) in Videos 1 and 2, and  $L = 40 L_{\text{diff}}$  (128 simulation cells) in Videos 3 and 4. For more information on EPAPS, see <http://www.aip.org/pubservs/epaps.html>.
- [16] V. Casagrande, Doctoral thesis, Technical University, Berlin, 2006, <http://opus.kobv.de/tuberlin/volltexte/2006/1273/>.
- [17] D. Walgraef, *Spatio-Temporal Pattern Formation* (Springer, Berlin, 1997).
- [18] A. M. Zhabotinsky, M. Dolnik, and I. R. Epstein, *J. Chem. Phys.* **103**, 10306 (1995).
- [19] Diffusion perpendicular to the plane is considered as dilution within a layer of effective thickness  $\approx l_{\text{diff}}$ .
- [20] B. Hess, A. Boiteux, and J. Krüger, *Advances in Enzyme Regulation* **7**, 149 (1969).
- [21] H. Hess and G. D. Bachand, *Mater. Today* **8**, 22 (2005).
- [22] H. R. Petty, R. G. Worth, and A. L. Kindzelskii, *Phys. Rev. Lett.* **84**, 2754 (2000).